Full scale experimental tests to evaluate the train slipstream in tunnels

S. Negri [*], G. Tomasini, P. Schito, D. Rocchi

Department of Mechanical Engineering, Politecnico di Milano, Italy

A B S T R A C T

The train slipstream, i.e. the air velocity induced by the train, is one of the most important aerodynamic effects connected to railway vehicles because it has a direct impact on the safety of passengers on the platform and track workers along the railway line. In recent years, a lot of studies were performed to understand the development of this phenomenon in open field, and specific EU standards, the EN 14067–4 and the TSI were issued. Instead, only few studies have been carried out to analyse the train slipstream in confined spaces (as tunnels, line sections with acoustic barriers, etc.), even though the first results of these analyses have shown that the confinement of the air causes more severe conditions regarding the speed of the air flow. This work aims at studying, through a full-scale experimental campaign, the effects on the air flow speed caused by the train passage. The effects of different train parameters (i.e. train type and length, etc.) and infrastructure parameters (i.e. geometry variations) were analysed. Lastly, the results of a specific test considering the presence of a stationary train inside the tunnel while another train is passing are described, to simulate scenarios of ordinary railway traffic.

1. Introduction

The train slipstream, i.e. the air velocity induced by the train, is one of the most important aerodynamic effects connected to railway vehicles because it has a direct impact on the safety of passengers on the platform and track workers along the railway line. Nowadays, thanks to the technological development of both trains and railway infrastructures, the transit speeds of trains can be very high; consequently, the gusts generated in the train slipstream can be very fast and potentially dangerous. The rolling stock TSI standard (RST TSI, 2008) currently allows to homologate trains, in relation to the slipstream phenomenon, by a test carried out in open air, but no specific indications are provided to the railway infrastructure manager to evaluate the maximum allowable velocities in confined spaces (i.e. underground station) to avoid to overcome the limit air speed values associated with the slipstream phenomenon.

Due to the need to study the slipstream phenomenon for the safety of passengers and workers on the line, in the past years, different research groups carried out many analyses in open field but only few of them focused on the development of this phenomenon in confined spaces.

In open field, in particular, the effects of different types, lengths or configurations of trains on the slipstream velocities were studied. For instance, Suzuki et al. (1996) performed a 3D CFD simulation to study the unsteady flow around a high-speed train and the induced yawing

moment fluctuation of the tail car. To determine the structure of the slipstream and wake of a high-speed train, Baker et al. (2001) carried out an experimental work using a 1/25th scale model of a four-coach train on a moving model rig (MMR); tests were carried out at different model speeds, with and without the simulation of a crosswind. Johnson et al. (2004) reported a collection of studies on high-speed trains slipstream carried out in a European research project (RAPIDE project), including full-scale tests, reduced-scale tests, CFD analysis and introducing a simplified human response modelling to the slipstream gusts. Sterling et al. (2008) described the results of full-scale and scaled models tests to analyse the different slipstream generation for passenger trains and freight trains. These studies led to the development of the TSI standard (Technical Specifications for Interoperability) (RST TSI, 2008) for the characterization of the vehicle during the train homologation phase. Over the past decade, further research in open air includes the analysis of the slipstream phenomenon by using scaled models, full-scale tests and CFD analysis. Considering the testing methodology with moving model rigs, the effect of train type, length and of the measurement position on the slipstream of freight trains were analysed by Soper et al. (2014), while Bell et al. (2015) analysed the slipstream of a high-speed train with the view of applying the reduced scale methodology for checking TSI compliance in the design phase of a train. Wind tunnel tests were performed by Bell et al. (2014, 2017) to assess the slipstream and wake of high-speed trains. Rocchi et al. (2018) and Soper and Baker,

---

2020 performed full-scale experimental campaigns to study the wind effects induced by passenger and freight trains pass-by in open air, while Zampieri et al. (2020) used full-scale data to perform a numerical-experimental analysis of the slipstream. Hemida et al. (2014), Maleki et al. (2017), Wang et al. (2017) and Flynn et al. (2014) tested the ability of URANS, DES, LES simulation and different turbulence models to reproduce the train slipstream.

Muld et al. (2012, 2014) simulated the slipstream of high-speed trains with different lengths, Wang et al.,(2018a, 2018b) studied the effect of the ground condition and of bogies on high-speed train slipstream and wake and Dunlop and Thompson (2022) investigated the possibility di reducing peak slipstream velocities through the implementation of angled fins or swirling flow injection.

The study of the slipstream effect in confined spaces, however, has been mainly developed on scaled models and with with CFD analyses. Gilbert et al. (2013) analysed the effects of different closed or partially closed infrastructure types by using moving model rigs, highlighting the main differences between the slipstream generated in open and closed environments, while Meng et al. (2019) made moving model tests to study the slipstream caused by a metro train passing through a tunnel. CFD numerical simulations on the wind field generated inside confined spaces were made by Khayrullina et al. (2015) on passenger and freight trains traveling inside a tunnel, also analyzing the most critical locations on the platform with respect to each train type. Using the same numerical approach, Fu et al. (2017) studied the most influential parameters, such as train and tunnel length, with respect to the slipstream. Iliadis et al. (2020) reproduced with numerical simulations the separated flow around freight trains passing through tunnel using a sliding mesh approach. Further numerical investigations were made to study the effect of different train/tunnel geometries or to reproduce two trains passing each other in a tunnel (LI and LIU (2017, 2020); Liu et al. (2023); Meng et al. (2021); Xiong et al. (2022)). These studies allowed to notice a difference between the slipstream generated in the open field and in confined spaces, which depends not only on the train parameters but also on those related to the infrastructure. Nowadays, however, to the best of the authors' knowledge, there are no confined space slipstream analysis based on full scale experimental tests performed on conventional railway lines, hence it can be quite difficult to perform a complete analysis with an adequate number of train passages, as suggested by the TSI, and to develop or update regulations related to the aerodynamic phenomenon generated in closed infrastructures like tunnels.

This paper aims to analyse the main characteristics of the slipstream phenomenon inside a tunnel, to understand if the phenomenon generated by a train passing through a tunnel is qualitatively equivalent to that generated in open field and to identify the most significant parameters by using a full-scale measurements data set. The experimental setup adopted for the full-scale experimental campaign carried out in an Italian railway underground station is described in *Section 2*. The data obtained from the experimental campaign are analysed in *Section 3* and the main parameters that influence the flow development inside the tunnel and their effects are shown, considering the air flow generated before the train arrival, the traveling speed, the different types and lengths of trains and the effect of local geometry variations of the infrastructure; in addition, to study the influence of the measurement position two different measurement locations from the railway track center are considered. Lastly, a specific test considering the presence of a stationary train inside the tunnel while another train is passing, in order to simulate scenarios where a train runs beside a still train, will be described at the end of *Section 3*. In *Section 4* are summarized the conclusions and a brief overview of the future work, including a numerical CFD model validation and its use.

2. Experimental setup and train typologies

A full-scale experimental campaign was performed in an underground station in Italy, to measure the air speed generated by the rolling stock circulating on the line, i.e. conventional passenger trains, high-speed trains and freight trains. Fig. 1 shows the entrance and the internal geometry of the tunnel, to give a better understanding of the tunnel's shape and dimensions. Fig. 2 shows the experimental setup adopted during the experimental campaign.

For the slipstream velocity measurement, two GILL Instruments WindMaster 3-Axis ultrasonic anemometers, with maximum sampling frequency of 32 Hz and measurement uncertainty about 0.2 m/s, were placed along the line inside the tunnel, 1.2 m high from the platform (according to the TSI standard (2008)) and at 2.5 m (the closest allowed position for the passengers) and 3 m from the track centres. In particular, it was chosen to place an anemometer near the narrowing of the platform (on the odd track side) and another anemometer at the typical section of the platform (on the even track side). In addition to the anemometers, other instruments were used to allow a complete characterization of the slipstream. Three gates of photocells were installed to estimate the train's speed and length and to distinguish between different train types: two gates inside the tunnel allowed the train speed calculation by knowing the gates distance (166 m) and the time of the train nose (or tail) passing through the gates; performing the ratio between the gates distance and the passage time it was possible to obtain the mean train speed inside the tunnel. By knowing the train speed inside the tunnel and the train passage time, recorded by a single photocell gate, it was possible to estimate the train length for each passage. Furthermore, the train speed in an open area near the tunnel exit was estimated, exploiting an external photocells gate. The presence of three different gates was necessary to calculate the train's speed both inside and outside of the tunnel, to correctly evaluate the mean speed inside the tunnel in case of accelerating/decelerating train motion.

The system was designed to start the acquisition and recognize the vehicle type automatically as each train passes. The acquisition system was triggered by the signal of accelerometers located in the internal part of the tracks, after proper calibration of the threshold (set at 0.5 g) that allows to detect the passage of a train. The accelerometers were put in two different locations to catch the train arrival independently from the traveling direction (even or odd track directions) and the acquisition system was programmed to record from 10 s before the trigger time, up to 60 s after the same signal, obtaining an overall time history of 70 s for each train passage. The accelerometers have also been used to measure the number of axles of each carriage, to facilitate the distinction of each train type. The axles counting was performed by considering a threshold value, previously calibrated, on the acceleration signal to identify each axle passage. In order to have a precise train recognition system, based not only on train speed, carriage length and number of axles, a camera was positioned outside the tunnel on a catenary pole to acquire a video for each passing train. The video was acquired automatically by a computer program leveraging on the data acquisition triggering system. In Fig. 3, a snapshot from a video relating to a high-speed train passage is shown as an example of the camera acquisitions. All the measurement instruments were connected to an acquisition system composed by a computer with a programmable software and data acquisition cards and chassis.

For a better characterization of the train types and of the blockage ratio for each train, the drawings of the high-speed, conventional passenger and freight trains are shown in Fig. 4 - (a), (b) and (c) respectively. Moreover, in Table 1, the information regarding train length, number of cars, cross-sectional area and blockage ratio $\left(\frac{A_{train}}{A_{tunnel}}\right)$ are added, considering that the tunnel cross-section in the measurement area corresponds to 84 m^2.

4. Analysis of experimental data

The slipstream phenomenon will be analysed by plotting the ensemble averages of the wind velocity acquisitions for many passages

Fig. 1. Overview of railway tunnel: north entrance (a) and internal geometry near the platform (b).
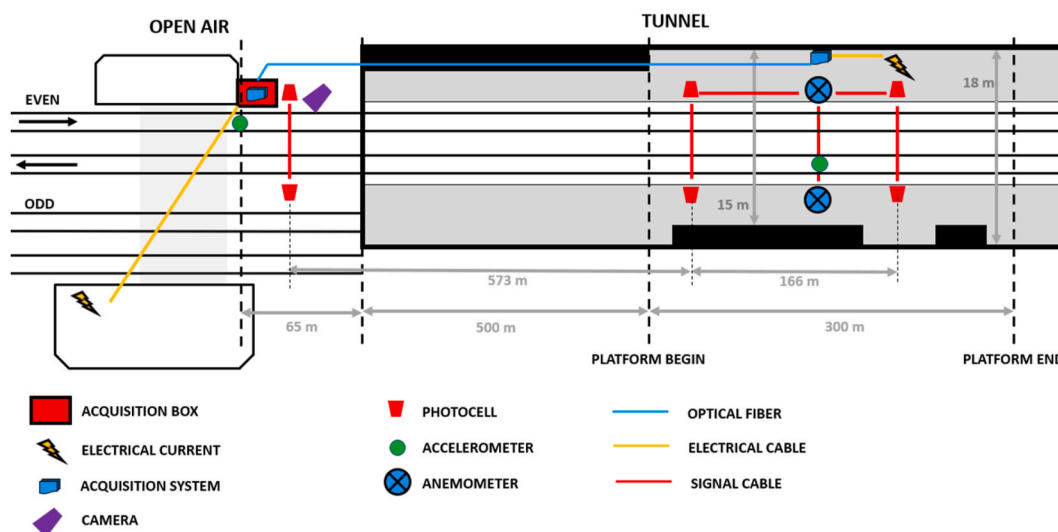

Fig. 2. Experimental set-up: open air and internal measurement stations for both the even and odd track directions.

Fig. 3. Snapshot from an acquired video from the camera: ETR1000 high-speed train about to enter the tunnel.

of the same train type performing the ensemble averaging technique, by following the procedure described in Baker et al. (2014). All the wind histories were aligned with space $x = 0\ m$ to a common position, which in this study is considered as the train nose passage in front of the anemometers. The ensemble curves allow to appreciate the run-to-run variation by considering the standard deviation values (σ_{U_x}), but also similar slipstream trends, where present, can be successfully

highlighted. For the overall analysis, the measured vertical velocity components were small and only the longitudinal component of the horizontal velocities - which represent the main contribution of the slipstream velocity - will be presented. In Fig. 5 -, different slipstream profiles obtained from 20 high-speed train passages and the ensemble mean and standard deviation curves, superposed in the same graph, are reported. By analysing this figure, it is possible to notice that the air flow inside the tunnel is perturbed by the train even before the train nose passes at the measurement position: an almost linear increase of the longitudinal air velocity (U_x) can be observed before the train passage ($x = 0\ m$), while in open space the air velocity measured before the train passage is not perturbed by the train itself, but presents fluctuations only due to the ambient air variation (Rocchi et al. (2018); Sterling et al. (2008)). Hence, to describe the slipstream in confined field, it is chosen to split the analysis into two parts: the air variation before the train passage at the measurement location, in *Section 3.1*, and the slipstream behaviour during and after the train passage, in *Section 3.2*. Moreover, as the train speed variations result in different slipstream profiles and taken into account that during the runs measured inside the tunnel the trains do not usually travel at the same velocity, the train speed effect on the air flow characteristics is deleted by scaling the air speed to a specific reference train velocity, similarly to the procedure described in the EN 14067-4 Standard (CE, 2009) for the analysis of the maximum air speed for different passages. Moreover, In Baker et al. (2014) and Soper et al.
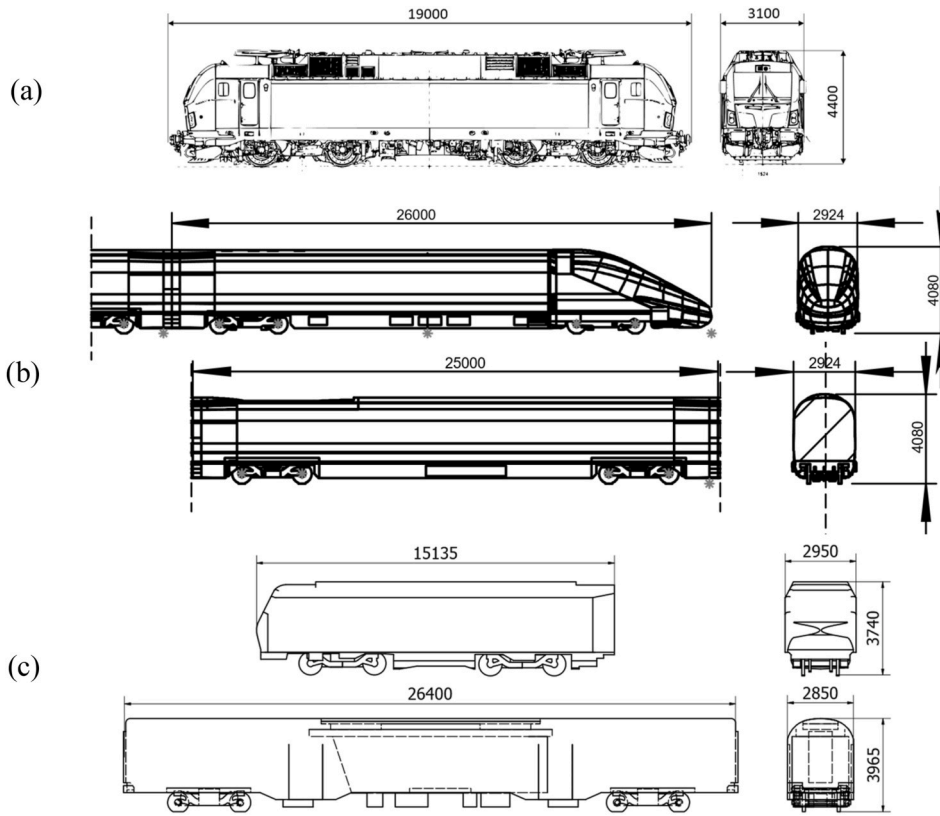
Fig. 4. Trains dimension and shape for freight (a), high-speed (b) and conventional passenger trains (c).

Table 1
Train length, number of coaches, frontal area and blockage ratio for each train type.

Train type	Train length [m]	N. cars (locomotive included)	Train cross-sectional area [m^2]	Blockage ratio ($\frac{A_{train}}{A_{tunnel}}$)
High speed	202	8	10.9	0.13012
Conventional (E464 locomotive)	60<L < 300	3<n < 12	11.9	0.14205
Freight	200<L < 600	10<n < 36	~12 (for the locomotive, similar to E464 model)	0.14325

(2014) the measured slipstream velocities were normalised by train speed during the ensemble averages analysis, showing a linear relationship with respect to train speed for velocity data. Therefore, in the present analysis, each time-history of the air speed (U_{air}) is re-scaled, by applying the following formula in Equation (2), to relate each measurement to the reference train speed:

$$U_x = \frac{U_{air}}{V_{train}} \, V_{ref} \qquad (2)$$

where V_{train} corresponds to the train traveling speed measured at the specific time-history. Three different reference speeds (V_{ref}), one for each train type, are considered:

- 160 km/h for high-speed trains;
- 145 km/h for conventional trains;
- 120 km/h for freight trains.

3.1. Air flow behaviour before train passage

The phenomenon which causes the air inside the tunnel to move even ahead of the train itself is related to a pushing action generated by the train entering and traveling in the confined space and is usually named *piston effect*. Depending on the volume occupied by the train and on its geometry, this phenomenon causes an air speed-up which develops mainly in longitudinal direction. To better understand the piston effect, the phenomenon is studied with the ensemble averaging technique:

- for three train categories: high-speed trains (*ETR*1000), conventional passenger trains and freight trains;
- for the same train type with different lengths.

In Fig. 6, the slipstream profiles of high speed, conventional and freight trains having similar lengths (about 200 m) and comparable blockage ratio, with respect to the tunnel cross-section (refer to Table 1), are shown in terms of ensemble means of the longitudinal air velocity ($\overline{U_x}$) while in Table 2 the characteristics of the three train groups are summarized.

Taking into account possible differences caused by train lengths and blockage ratios, that are not exactly matching, and considering the three different speeds with which the slipstream profiles are rescaled for the three train types, from the results it can be appreciated how freight trains seem to cause a higher piston speed.

To be noted, however, that by rescaling the slipstream curves of freight trains with a lower speed than that of high-speed trains, the authors are aware that the possible worsening effect given by blockage/drag is less worsening than it could be if all trains were running at the same speed. However, the main objective of this study is not the evaluation of the slipstream speeds under the same conditions for each train, but the evaluation of the actual passing conditions in this environment, i.e. different maximum allowed traveling speeds.
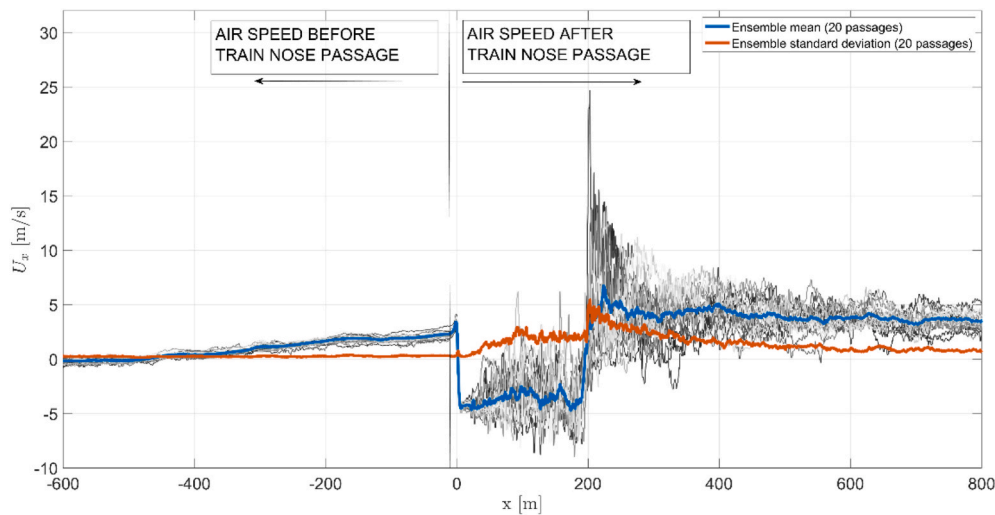
Fig. 5. Longitudinal air flow velocity in tunnel, before and after train nose passage. Different slipstream profiles are reported in grey scale; the ensemble mean and standard deviation curves are superimposed in coloured profiles.
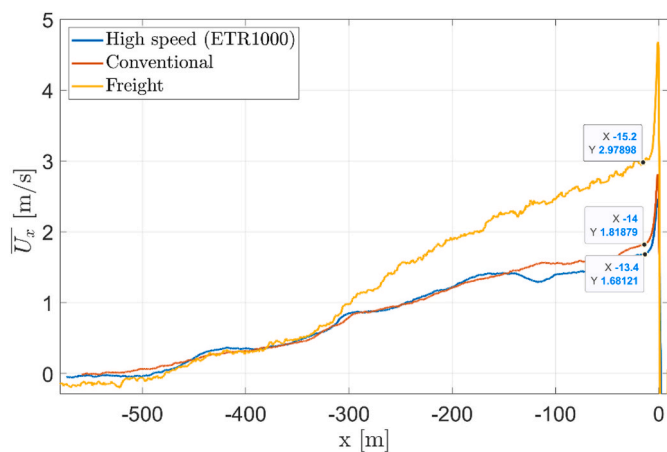

Fig. 6. Piston effect, different train types. On x axis: train nose position from anemometers, on y axis: ensemble mean of longitudinal air speed.

Fig. 7. Piston effect, different train lengths. On x axis: train nose position from anemometers, on y axis: ensemble mean of longitudinal air speed.

Table 2
Piston effect: train type, length, track direction, number of considered passages and lateral measurement position.

Train type	Train length [m]	Track direction	Number of passages	Measurement position from track center [m]
High speed	202	Even	25	2.5
Conventional	~200	Even	35	2.5
Freight	~200	Even	9	2.5

To study the effect of train length, three groups of conventional passenger trains having different lengths are compared. The resulting averaged slipstream profiles, reported in Fig. 7 as ensemble means, prove that the train length represents another influence parameter on the air speed inside the tunnel. Because of the greater volume occupied by longer passenger trains, the final ramp velocity generated before the train arrival results higher for the longest trains.

Therefore, it is possible to conclude that the flow acceleration before the train passage, caused by the piston effect, mainly depends on the train volume. All trains entering in the tunnel show an almost linear increase of the air speed before the train passing, reaching higher speed values for longer trains with a greater surface roughness.
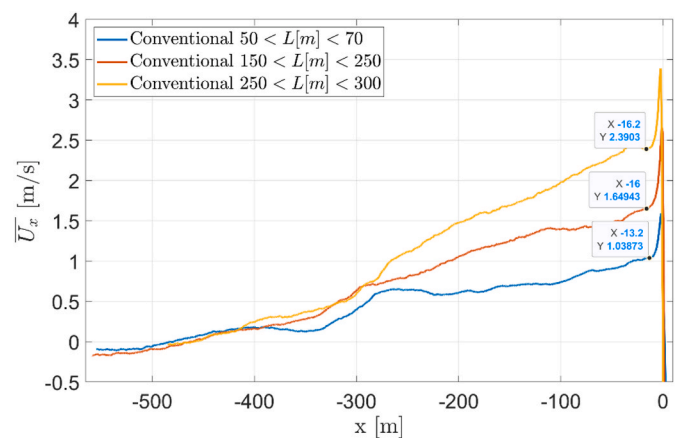
In Section 3.2, the speed value due to the piston effect before the train arrival will be subtracted from the slipstream profiles, in order to study the effects of the parameters on the two parts of the profile separately (before and after the train passage).

3.2. Air flow behaviour after the train passage

Considering the air flow development during and after the train passage in front of the anemometers, the effects of the main parameters related to both, train and infrastructure characteristics, are analysed in this section.

3.2.1. Train type effect

In this section, the comparison between the slipstream generated by different train types, having the same length of about 200 m,[1] is analysed. All the characteristics of the train groups considered for the sensitivity analysis are summarized in Table 3.

The ensemble mean profiles generated by the three train types traveling on the same railway side (odd track side of the tunnel), plotted in Fig. 8, show that the behaviour of high-speed trains and the

---

[1] This reference length was selected because high-speed trains passing through the railway station are all 202 m long.

Table 3

-Train type effect: train type, train length, reference speed, platform direction, number of considered passages and lateral measurement position.

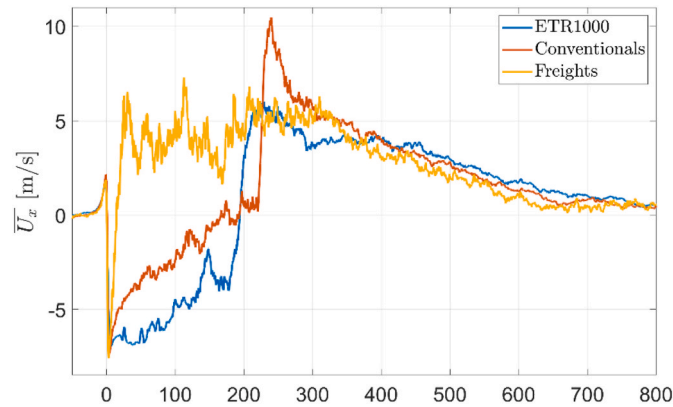| Train type	Train length [m]	Reference speed [km/h]	Track direction	Number of passages	Measurement position from track centre [m]
High speed	202	160	Odd	34	2.5
Conventional	~200	145	Odd	42	2.5
Freight	~200	120	Odd	13	2.5

Fig. 8. Train type comparison (Length = 200m), odd track direction. On x axis: train nose position from anemometers, on y axis: ensemble mean of longitudinal air speed.

Fig. 9. Train type comparison (Length = 200m), odd track direction. On x axis: train nose position from anemometers, on y axis: ensemble standard deviation of longitudinal air speed.

Fig. 10. Tunnel cross section scheme at the measurement position.

conventional passenger trains is similar, noting that the maximum air speed is reached in the near wake zone. Considering these two train types, taking into account variations related to slight differences between blockage and train length and considering the three different re-scaling speeds which are applied in the study, it can be considered that higher flow speeds are generated by the conventional trains due to their less aerodynamically optimized shape. For freight trains, the slipstream profile is different from the other two types: the irregular and discontinuous composition of the convoys does not allow the growing of a boundary layer along the train and the consequent formation of a persistent back flow after the train nose passage. For this train type, the highest speed peaks are generated, regardless of transit speeds, in the nose and boundary layer regions. The exact peak position is however dependent on the specific train configuration and carriages type, which could be very different in terms of dimension and shape, making it very difficult, for freight trains, to find a generalized trend.

Considering the region after the near wake zone, the slipstream velocity tends to decrease for all the train types in a similar way, showing that the slipstream lasts for many seconds after the train passage: in spatial domain, as represented in the figure, it is possible to notice that the slipstream could be considered over about 700 m after the train nose passage (so when the nose is 700 m further in the tunnel).

In Fig. 9 the ensemble standard deviation curves for the three train types are reported, showing once again the highest variability for freight trains in all the slipstream zones, particularly in the boundary layer zone, between 0 m and 200 m. For high-speed and conventional trains, the ensemble standard deviation curves have a similar behaviour: lower values are shown in the first part of the boundary layer zone, due to a more deterministic behaviour of these trains during the nose passing and the boundary layer formation, while after this point the standard deviation values increase near the train end at x = 200 m.

3.2.2. Platform effect

The railway tunnel does not have a symmetrical section in the platform area: Fig. 10 shows a scheme of the cross section of the station
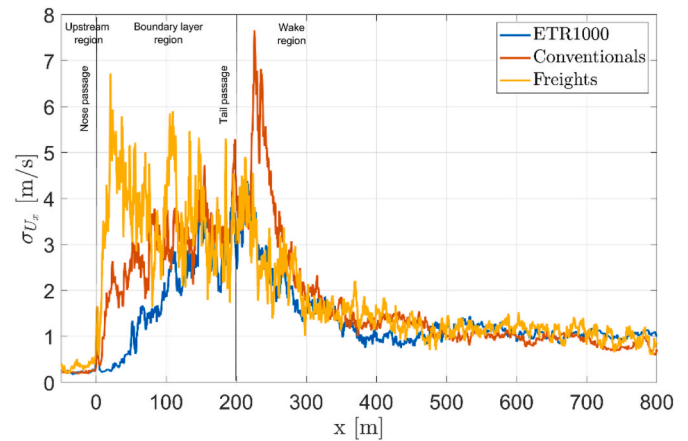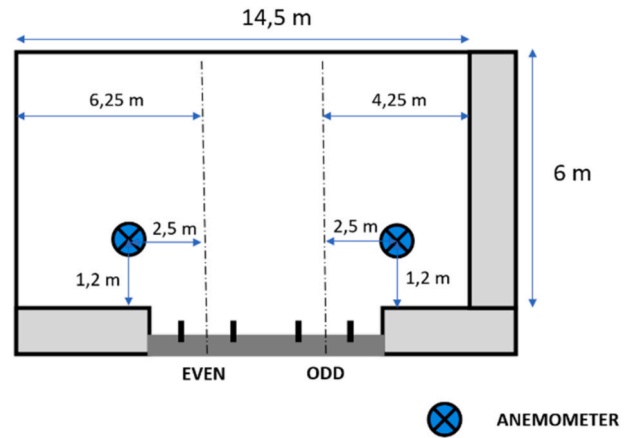
at the measurement position: it is possible to notice that, at the anemometer's location, the odd tunnel side is narrower with respect to the even one of about 2 m. To assess possible differences caused by the tunnel local geometry, the slipstream generated inside this confined space was analysed separately for the even and odd track sides.

For the analysis high-speed trains and conventional passenger trains are considered and a lateral position of the anemometer equal to 2.5 m from the centre of the rails, as reported in Table 4 together with the train groups characteristics. Following the analysis procedure described in Equation (2), all the spatial histories of the longitudinal air speed have been re-scaled by considering the reference speeds of each train type.

Figs. 11 and 12 shows, respectively for high-speed and conventional

Table 4

Tunnel platform effect: train type, train length, reference speed, platform direction, number of considered passages and lateral measurement position.

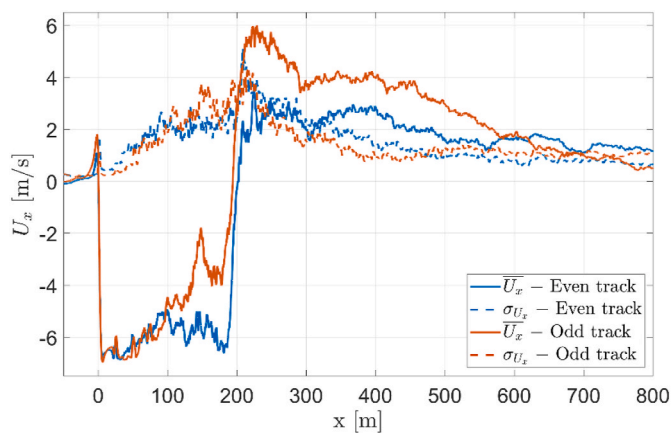| Train type	Train length [m]	Reference speed [km/h]	Track direction	Number of passages	Measurement position from track centre [m]
High speed	202	160	Even	32	2.5
High speed	202	160	Odd	34	2.5
Conventional	150<L < 250	145	Even	35	2.5
Conventional	150<L < 250	145	Odd	42	2.5

Fig. 11. Platform effect, high-speed trains. On x axis: train nose position from anemometers, on y axis: ensemble mean and standard deviation of longitudinal air speed.
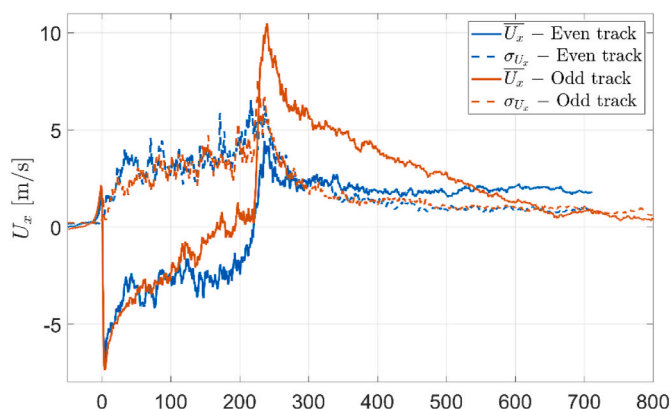

Fig. 12. Platform effect, conventional trains. On x axis: train nose position from anemometers, on y axis: ensemble mean and standard deviation of longitudinal air speed.

trains, the ensemble mean and standard deviation profiles: it is possible to observe higher slipstream velocities in the odd side of the tunnel. The air speed profiles recorded on this part of the tunnel present higher peaks in the nose and wake region for both train types, showing the greater speed increase right after the train tail passage.

This result is caused by a narrowing of the tunnel cross section in this zone, which creates a greater confinement of the flow. The local geometry on the odd side generates a slipstream profile which has shown to be different from the one generated on the even side, hence, a strong influence of the local infrastructure geometry on the slipstream generation was highlighted. Those conclusions are in agreement with the tests made with the moving model rig performed by Gilbert et al. (2013), where the train models were moved inside different types of infrastructures, as lateral barriers or closed/partially closed tunnels of different lengths, proving the influence of the infrastructure type and of the local geometrical variations on the slipstream velocities.

3.2.3. Train length effect

As reported in Section 3.1, one of the effects of the train length (L_{train}) when trains are traveling inside tunnels is related to the piston effect. However, the piston effect is not the only effect that could be affected by the train length variations, so a detailed analysis is now performed on the conventional passenger trains and on the freight trains, which could have different lengths depending on each configuration.

For the analysis, the ensemble mean and standard deviation curves were obtained by considering the train passages on a single track

direction for each train type, as reported in Table 5 with all the train groups characteristics. The number of passages used to calculate the ensemble average for each group is different, but for conventional trains there are at least 15 passages per group; on the other hand, for freight trains, the passages are highly uneven in terms of type and therefore the useful ones are significantly lower.

Starting from the conventional passenger train analysis, by organizing the trains in four different length groups, the results in terms of ensemble means are reported in Fig. 13. From these profiles, two main peculiarities have been noted: for shorter trains, the boundary layer can not reach a stability condition, which is reached after a specific length (about 100 m for this type of conventional trains). Moreover, longer trains show slightly higher velocity peaks in the tail/wake region, with respect to shorter ones.

As for the study made for conventional passenger trains, a collection of passages was analysed also for freight trains. Unlike conventional passenger trains, the slipstream profiles for the freights present a higher heterogeneity, because of the lower number of passages that were acquired for each length and in particular because of the higher variability due to the carriages shape and dimension. However, analysing the measured data shown in Fig. 14, similar considerations to those already made for conventional trains can be made about the dependency of the boundary layer stability. For freight trains, the maximum peak is recorded for intermediate-length trains in the boundary layer area. The small size of the sample considered certainly influences the position of the maximum (the ensemble average with fewer passages generates higher peaks). In any case, even for freight trains, an average growth of the slipstream is observed in the boundary layer area, therefore the average trend is consistent with that found for conventional trains.

3.2.4. Measurement position effect

During the campaign, the possibility to change the anemometers position in the tunnel was exploited to understand how the slipstream develops around the train, during its passage. In the first part of the campaign, the anemometers were positioned at a lateral distance of 2.5 m from the railway track centre, while in the second part they were moved to a greater lateral distance of 3.0 m from the track centre, maintaining the same height from the platform ground (1.2 m). In this section the effects of the position change are analysed for one train type only, the *ETR1000* high-speed train. In Table 6 are reported the main train groups characteristics.

From the ensemble analysis, the results in terms of the mean and standard deviation of slipstream velocities are shown in Fig. 15 for the passages on the even track side of the tunnel.

From the results, it can be inferred that the slipstream velocities change according to the measurement position. At the train nose

Table 5
Train length effect: train type, train length, referencespeed, platform direction, number of considered passages and lateral measurement position.

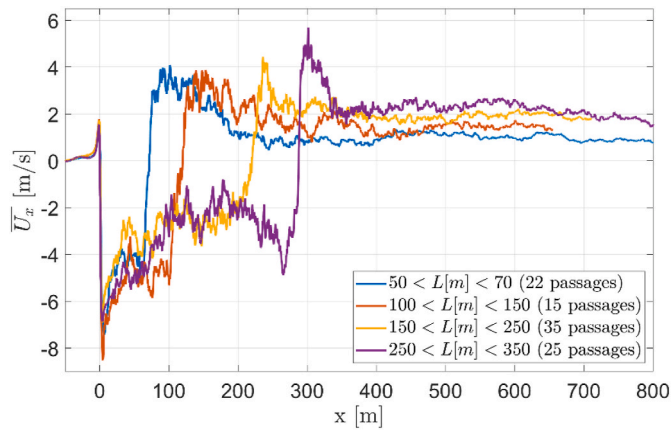| Train type	Train length [m]	Reference speed [km/h]	Track direction	Number of passages	Measurement position from track center [m]
Conventional	50<L ≤ 70	145	Even	22	2.5
Conventional	100<L ≤ 150	145	Even	15	2.5
Conventional	150<L ≤ 250	145	Even	35	2.5
Conventional	L > 250	145	Even	25	2.5
Freight	L < 250	120	Odd	13	2.5
Freight	250<L ≤ 400	120	Odd	8	2.5
Freight	400<L ≤ 600	120	Odd	12	2.5

Fig. 13. Length effect, conventional trains, even direction. On x axis: train nose position from anemometer, on y axis: ensemble mean of longitudinal air speed.
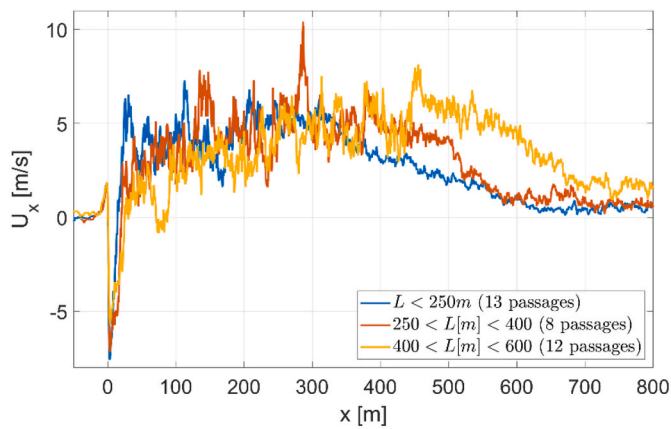

Fig. 14. Length effect, freight trains, odd direction. On x axis: train nose position from anemometer, on y axis: ensemble mean of longitudinal air speed.

passage, the measured velocity peak is higher at 2.5m than that at 3.0 *m* from the track centre, because the greater distance from the train allows the air to slow down before reaching the anemometer. Anyway, the most significant difference between the two measurement positions can be noted in the boundary layer zone: in the first part of it, up to about 25 *m* from the train nose (x = 0 *m*), the boundary layer development is equivalent for the two measurement positions. In the next section, between 25 *m* to 100 *m*, the air flow at the 3.0 *m* is speeding up, while the one at 2.5 *m* shows an opposite trend. This behaviour can be explained by considering the boundary layer development between the train side and the tunnel walls, as shown in Fig. 16: close to the train, the air tends to go in a positive direction (the same direction as the train), while near the walls, a back flow is generated by the piston effect. Considering the two measurement positions, it is possible to justify the higher back flow velocity measured at the 3.0 *m* lateral position.

3.2.5. Worsening condition: presence of a stationary train inside the tunnel

In order to simulate scenarios where a train runs beside a still train,

situation which usually happens in standard railway stations, a specific test has been designed and performed. In particular, a conventional passenger train has been kept still on the railways even track, while on the other railway track a train (equal to the stationary one) is allowed to circulate on the line at conventional traveling speed and in both the directions on the odd railway track, acquiring three passages for each direction. The presence of an additional train on the line represents a more critical condition with respect to single-train passage, because the still train generates a significant reduction of the section (and volume). A layout of the tunnel with the still train is reported in Fig. 17.

In order to make a comparison with the slipstream profiles obtained from this test, conventional passenger trains with the same length of the stationary train were searched in the data set, paying attention to choose the passages measured with the same anemometers lateral distance (3.0 *m* from the track centre) considered for the stationary train test.

In Fig. 18, the slipstream profiles obtained from the passages of conventional passenger trains of the same length (300 m), at the equivalent measurement point (3m from track centre) and running in the same direction (odd) are shown.

From the results, reported in Fig. 18 for the odd track direction some features induced by the presence of the still train can be noted; only the passages in the odd track direction are considered for the comparison because the moving trains are circulating on the odd side of the tunnel, while the stationary train is positioned on the even side. Unlike in the previous paragraphs of *Section 3.2*, all the phenomena which characterize the slipstream are included in this analysis to permit a significant comparison between the two cases; so the piston effect, related to air the speed up before the train arrival, was maintained in the slipstream profiles.

The results in Fig. 18 show that the presence of the stationary train on the line causes worse flow conditions, especially in the nose and near wake regions. Moreover, it is possible to notice an additional phenomenon induced by the presence of the stationary train: between 90 *m* and 120 *m* after the train nose passage, the air flow suddenly shows a change in its velocity, while after this zone the air speed returns to be similar to the slipstream trend caused by the boundary layer development without
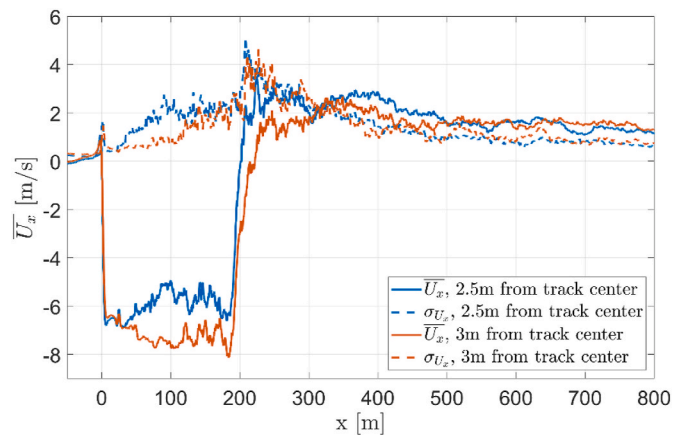

Fig. 15. Measurement position effect, high-speed trains, even track. On x axis: train nose position from anemometer, on y axis: ensemble mean and standard deviation of longitudinal air speed.

Table 6
Train length effect: train type, train length, referencespeed, platform direction, number of considered passages and lateral measurement position.

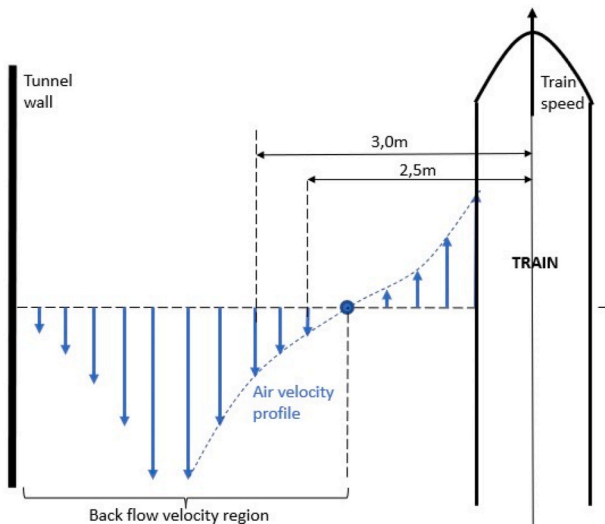| Train type	Train length [m]	Reference speed [km/h]	Track direction	Number of passages	Measurement position from track centre [m]
High speed	202	160	Even	32	2.5
High speed	202	160	Odd	34	2.5
High speed	202	160	Even	25	3.0
High speed	202	160	Odd	35	3.0

Fig. 16. Measurement position effect, longitudinal air speed distribution between the train and the tunnel walls.

the still train. By comparing the relative positions of the moving and still trains, it is possible to infer that the region in which the air speed decreases could be caused by the nose of the moving train that overtakes the still train end, creating a sudden volume increase that could be the reason of the air slow down. Other variations in air speed were sought, perhaps due to the passage of the nose or tail of the train moving in front of the stationary train: between 350 m and 400 m from the train nose passage, a fast decrease of the flow velocity is recorded. In this case, the velocity decrease could be due to the passage of the tail of the moving train next to the tail of the stationary train: this could generate a sudden change of section, which may cause this specific air velocity behaviour.

4. Conclusions

In this research, the full-scale experimental campaign carried out at a specific railway tunnel for the slipstream characterization in confined spaces was described. Referring to conventional passenger trains, high-speed trains and freight trains, the experimental campaign allowed to analyse the parameters that influence the development of the air flow inside the tunnels, related both to the train and to the infrastructure: train type, length and speed were considered as well as the train direction, to measure the flow velocity at two different lateral position from the railway track centre. In addition, a specific test was performed by considering the presence of a stationary train inside the tunnel while another train is passing, in order to simulate scenarios of railway traffic inside the stations.

Referring to the analyses carried out in the previous sections, the following conclusions can be drawn.

- The piston effect is acting inside confined spaces even before the train arrival at the station and is dependent on the train length and geometry. The most critical train types, regarding the speed up caused by the piston effect, are freight trains; because of their non-optimized shape and volume, they cause a significant air speed increase before the train arrival at the measurement position.
- The slipstream phenomenon generated by high-speed trains and conventional passenger trains in tunnel is similar, showing maximum peaks in the wake region. For freight trains, the slipstream profile is different from that associated to the other two types because of the discontinuous boundary layer growth. For freight trains, the highest peaks are generated in the nose and boundary layer regions.
- The study of the non-symmetrical geometry of the tunnel highlighted the highest slipstream velocities in the odd side of the tunnel, caused by the narrowing of the cross section in this area.
- As train length increases, higher speed peaks are generated within the tunnel; moreover, for shorter trains the boundary layer cannot reach a stability condition.
- Moving the anemometers away from the centre of the rails, from 2.5 m to 3 m, slightly lower slipstream maximum velocities are found, but a faster back flow velocity is measured.
- An additional test with a stationary train on the line was performed, noting greater velocity peaks for the runs where the stationary train was present in the line; hence, the need to consider also the railway traffic conditions for slipstream assessments was highlighted.

During the experimental campaign, the measurement stations were located not only inside the tunnel but also in an open field adjacent to the railway tunnel entry; in a successive paper, further analyses will be made to understand the main differences between the slipstream
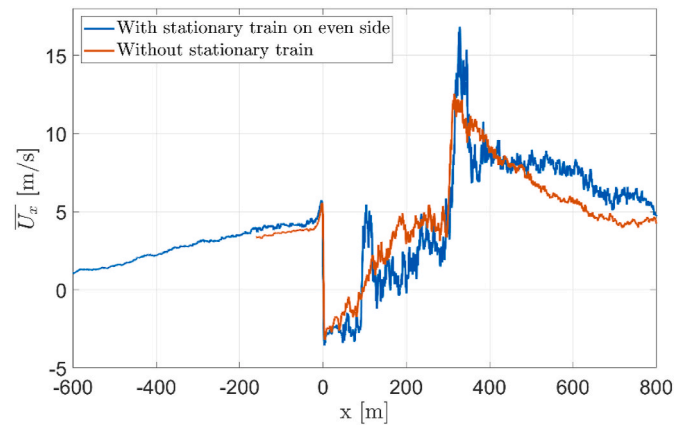

Fig. 18. Stationary train test: conventional trains, odd track. On x axis: train nose position from anemometer, on y axis: ensemble mean of longitudinal air speed.
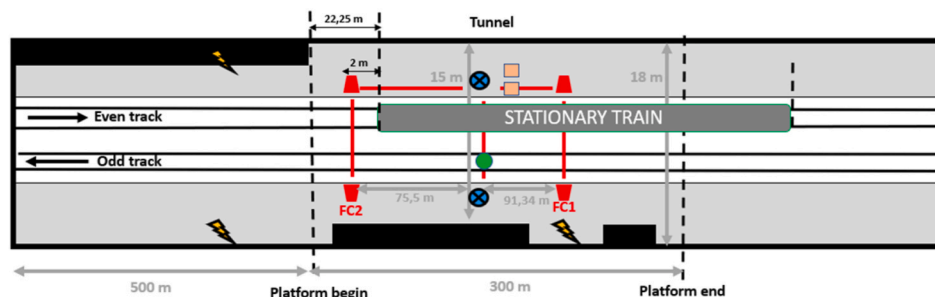

Fig. 17. Tunnel setup scheme for tests with a stationary train on the even track of the railway.

generated by the same trains in the open field and within the tunnel for the same collection of train passages.

In addition, as the slipstream development is dependent on the infrastructure geometry, a further study on tunnels with different cross sections and geometrical features should be performed to find which specific geometry causes the worst conditions in terms of wind speed. For this purpose, the data set coming from the experimental campaign could be used as a reference for a CFD model validation. The availability of a validated numerical model could potentially allow to determine the slipstream velocities for all tunnel types and in a continuous way inside the domain, without having to resort to more expensive experimental campaigns.

Credits

Stefano Negri:Conceptualization, Methodology, Software, Formal Analysis, Investigation, Writing - Original Draft. Gisella Tomasini: Writing - Review & Editing, Resources, Investigation, Visualization, Supervision.Paolo Schito: Resources, Investigation, Visualization, Supervision. Daniele Rocchi: Investigation, Supervision, Project Administration.

Declaration of competing interest

The authors declare that they have no known competing financial interests or personal relationships that could have appeared to influence the work reported in this paper.

Data availability

The authors do not have permission to share data.

Acknowledgments

References

Baker, C.J., Dalley, S.J., Johnson, T., Quinn, A., Wright, N.G., 2001. The Slipstream and Wake of a High-Speed Train.

Baker, C.J., Quinn, A., Sima, M., Hoefener, L., Licciardello, R., 2014. Full-scale measurement and analysis of train slipstreams and wakes. Part 1: ensemble averages. Proc. Inst. Mech. Eng. F J. Rail Rapid Transit 228 (5), 451–467. https://doi.org/10.1177/0954409713485944.

Bell, J.R., Burton, D., Thompson, M., Herbst, A., Sheridan, J., 2014. Wind tunnel analysis of the slipstream and wake of a high-speed train. J. Wind Eng. Ind. Aerod. 134 (1), 122–138. https://doi.org/10.1016/j.jweia.2014.09.004.

Bell, J.R., Burton, D., Thompson, M.C., Herbst, A.H., Sheridan, J., 2015. Moving model analysis of the slipstream and wake of a high-speed train. J. Wind Eng. Ind. Aerod. 136, 127–137. https://doi.org/10.1016/j.jweia.2014.09.007.

Bell, J.R., Burton, D., Thompson, M.C., Herbst, A.H., Sheridan, J., 2017. A wind-tunnel methodology for assessing the slipstream of high-speed trains. J. Wind Eng. Ind. Aerod. 166, 1–19. https://doi.org/10.1016/j.jweia.2017.03.012.

CE, 2009. Standard. "Railway applications aerodynamics-Part 4. In: Requirements and Test Procedures for Aerodynamics on Open Track". CEN EN14067-4.

Dunlop, J.A., Thompson, M.C., 2022. Reducing slipstream velocities experienced in proximity to high-speed trains. Fluid 7 (2). https://doi.org/10.3390/fluids7020072.

Flynn, D., Hemida, H., Soper, D., Baker, C., 2014. Detached-eddy simulation of the slipstream of an operational freight train. J. Wind Eng. Ind. Aerod. 132, 1–12. https://doi.org/10.1016/j.jweia.2014.06.016.

Fu, M., Li, P., Liang, X.F., 2017. Numerical analysis of the slipstream development around a high-speed train in a double-track tunnel. PLoS One 12 (3). https://doi.org/10.1371/journal.pone.0175044.

Gilbert, T., Baker, C.J., Quinn, A., 2013. Gusts caused by high-speed trains in confined spaces and tunnels. J. Wind Eng. Ind. Aerod. 121, 39–48. https://doi.org/10.1016/j.jweia.2013.07.015.

Hemida, H., Baker, C., Gao, G., 2014. The calculation of train slipstreams using large-eddy simulation. Proc. Inst. Mech. Eng. F J. Rail Rapid Transit 228 (1), 25–36. https://doi.org/10.1177/0954409712460982.

Iliadis, P., Hemida, H., Soper, D., Baker, C., 2020. Numerical simulations of the separated flow around a freight train passing through a tunnel using the sliding mesh technique. Proc. Inst. Mech. Eng. F J. Rail Rapid Transit 234 (6), 638–654. https://doi.org/10.1177/0954409719851421.

Johnson, T., Dalley, S., Temple, A., 2004. Recent Studies of Train Slipstreams.

Khayrullina, A., Blocken, B., Janssen, W., Straathof, J., 2015. CFD simulation of train aerodynamics: train-induced wind conditions at an underground railroad passenger platform. J. Wind Eng. Ind. Aerod. 139, 100–110. https://doi.org/10.1016/j.jweia.2015.01.019.

Li, W., Liu, T., 2017. Three-dimensional characteristics of the slipstream induced by a high-speed train passing through a tunnel. In: DEStech Transactions on Engineering and Technology Research. https://doi.org/10.12783/dtetr/icia2017/15673 icia.

Li, W., Liu, T., Chen, Z., Guo, Z., Huo, X., 2020. Comparative study on the unsteady slipstream induced by a single train and two trains passing each other in a tunnel. J. Wind Eng. Ind. Aerod. 198 https://doi.org/10.1016/j.jweia.2020.104095.

Liu, Z., Zhou, D., Soper, D., Chen, G., Hemida, H., Guo, Z., Li, X., 2023. Numerical investigation of the slipstream characteristics of a maglev train in a tunnel. Proc. Inst. Mech. Eng. F J. Rail Rapid Transit 237 (2), 179–192. https://doi.org/10.1177/09544097221100658.

Maleki, S., Burton, D., Thompson, M.C., 2017. Assessment of various turbulence models (ELES, SAS, URANS and RANS) for predicting the aerodynamics of freight train container wagons. J. Wind Eng. Ind. Aerod. 170, 68–80. https://doi.org/10.1016/j.jweia.2017.07.008.

Meng, S., Zhou, D., Wang, Z., 2019. Moving model analysis on the transient pressure and slipstream caused by a metro train passing through a tunnel. PLoS One 14 (9). https://doi.org/10.1371/journal.pone.0222151.

Meng, S., Li, X., Chen, G., Zhou, D., Chen, Z., Krajnovic, S., 2021. Numerical simulation of slipstreams and wake flows of trains with different nose lengths passing through a tunnel. Tunn. Undergr. Space Technol. 108 https://doi.org/10.1016/j.tust.2020.103701.

Muld, T.W., 2012. Slipstream and Flow Structures in the Near Wake of High-Speed Trains (Doctoral Dissertation. KTH Royal Institute of Technology).

Muld, T.W., Efraimsson, G., Henningson, D.S., 2014. Wake characteristics of high-speed trains with different lengths. Proc. Inst. Mech. Eng. F J. Rail Rapid Transit 228 (4), 333–342. https://doi.org/10.1177/0954409712473922.

Rocchi, D., Tomasini, G., Schito, P., Somaschini, C., 2018. Wind effects induced by high speed train pass-by in open air. J. Wind Eng. Ind. Aerod. 173, 279–288. https://doi.org/10.1016/j.jweia.2017.10.020.

RST TSI, H.S., 2008. Technical Specification for Interoperability Relating to the 'rolling Stock' Sub-system of the Trans-European High-Speed Rail System". Official Journal of the European Union L, 847132.

Soper, D., Baker, C., 2020. A full-scale experimental investigation of passenger and freight train aerodynamics. Proc. Inst. Mech. Eng. F J. Rail Rapid Transit 234 (5), 482–497. https://doi.org/10.1177/0954409719844431.

Soper, D., Baker, C., Sterling, M., 2014. Experimental investigation of the slipstream development around a container freight train using a moving model facility. J. Wind Eng. Ind. Aerod. 135, 105–117. https://doi.org/10.1016/j.jweia.2014.10.001.

Sterling, M., Baker, C.J., Jordan, S.C., Johnson, T., 2008. A study of the slipstreams of high-speed passenger trains and freight trains. Proc. Inst. Mech. Eng. F J. Rail Rapid Transit 222 (2), 177–193. https://doi.org/10.1243/09544097JRRT133.

Suzuki, M., Maeda, T., Arai, N., 1996. Numerical Simulation of Flow Around a Train, pp. 311–317. https://doi.org/10.1007/978-3-322-89838-8_41.

Wang, S., Bell, J.R., Burton, D., Herbst, A.H., Sheridan, J., Thompson, M.C., 2017. The performance of different turbulence models (URANS, SAS and DES) for predicting high-speed train slipstream. J. Wind Eng. Ind. Aerod. 165, 46–57. https://doi.org/10.1016/j.jweia.2017.03.001.

Wang, S., Burton, D., Herbst, A.H., Sheridan, J., Thompson, M.C., 2018a. The effect of the ground condition on high-speed train slipstream. J. Wind Eng. Ind. Aerod. 172, 230–243. https://doi.org/10.1016/j.jweia.2017.11.009.

Wang, S., Burton, D., Herbst, A., Sheridan, J., Thompson, M.C., 2018b. The effect of bogies on high-speed train slipstream and wake. J. Fluid Struct. 83, 471–489. https://doi.org/10.1016/j.jfluidstructs.2018.03.013.

Xiong, X., Cong, R., Li, X., Geng, Y., Tang, M., Zhou, S., Na, Y., Jiang, C., 2022. Unsteady slipstream of a train passing through a high-speed railway tunnel with a cave. Transport. Saf. Environ. 4 (4) https://doi.org/10.1093/tse/tdac032.

Zampieri, A., Rocchi, D., Schito, P., Somaschini, C., 2020. Numerical-experimental analysis of the slipstream produced by a high speed train. J. Wind Eng. Ind. Aerod. 196 https://doi.org/10.1016/j.jweia.2019.104022.